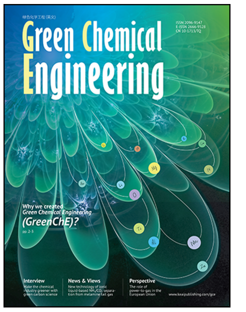

COSMO-RS screening of organic mixtures for membrane extraction of aromatic amines: TOPO-based mixtures as promising solvents

Gilles Van Eygen, Catherine Echezuria, Anita Buekenhoudt, João.A.P. Coutinho, Bart Van der Bruggen, Patricia Luis

PII: S2666-9528(24)00088-8

DOI: https://doi.org/10.1016/j.gce.2024.10.003

Reference: GCE 250

To appear in: *Green Chemical Engineering*

Received Date: 4 September 2024

Revised Date: 27 September 2024

Accepted Date: 14 October 2024

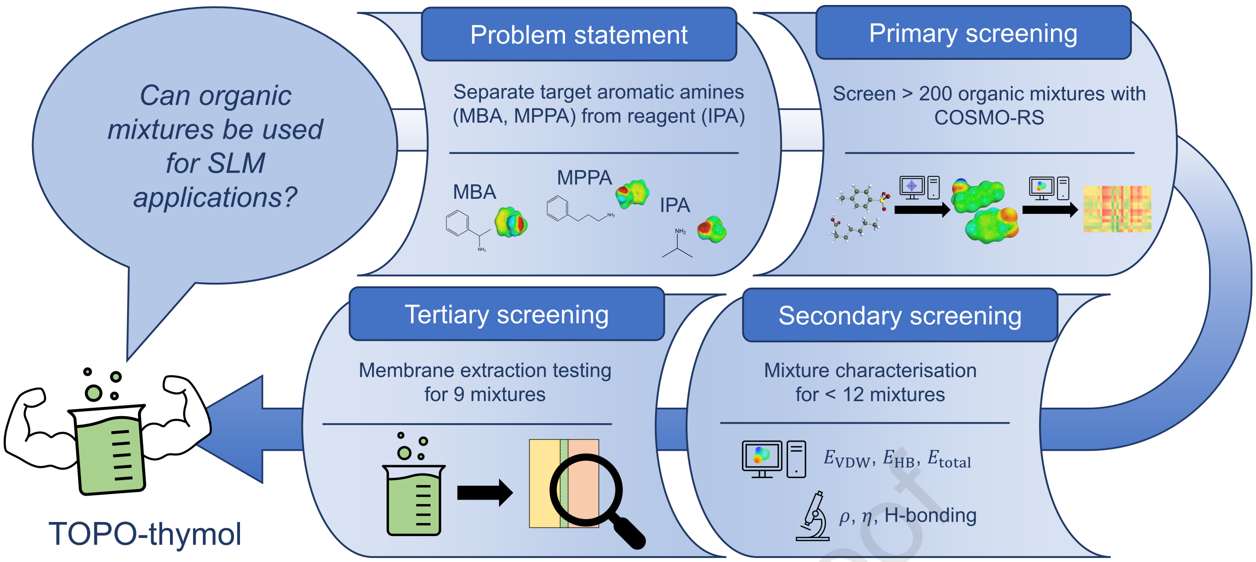
Can organic mixtures be used for SLM applications?
Problem statement
Separate target aromatic amines (MBA, MPPA) from reagent (IPA)
MBA
MPPA
IPA
Primary screening
Screen > 200 organic mixtures with COSMO-RS
Secondary screening
Mixture characterisation for < 12 mixtures
E_{VDW}, E_{HB}, E_{total}
ρ, η, H-bonding
Tertiary screening
Membrane extraction testing for 9 mixtures
TOPO-thymol

COSMO-RS screening of organic mixtures for membrane extraction of aromatic amines: TOPO-based mixtures as promising solvents

Gilles Van Eygen[a,b,c,*], Catherine Echezuria[b], Anita Buekenhoudt[c], João A.P. Coutinho[d], Bart Van der Bruggen[a], Patricia Luis[b,e]

a Process Engineering for Sustainable Systems (ProcESS), KU Leuven, Celestijnenlaan 200f, 3001, Leuven, Belgium

b Materials & Process Engineering (IMAP), Université catholique de Louvain, Place Sainte Barbe 2, B-1348, Louvain-la-Neuve, Belgium

c Unit Separation and Conversion Technology, Vlaamse Instelling voor Technologisch Onderzoek (VITO NV), Boeretang 200, 2400, Mol, Belgium

d CICECO-Aveiro Institute of Materials, Chemistry Department, University of Aveiro, 3810-193, Aveiro, Portugal

e Research & Innovation Centre for Process Engineering (ReCIPE), Place Sainte Barbe 2, bte L5.02.02, B-1348, Louvain-la-Neuve, Belgium

* Corresponding author: gilles.vaneygen@vito.be

Abstract

Aromatic amines are crucial in pharmaceuticals, but their synthesis is challenging due to unfavorable reaction equilibria and the use of costly, environmentally unfriendly methods. This study presents a membrane extraction (ME) process for *in situ* product removal (ISPR) of aromatic amines. Using a supported liquid membrane (SLM), α-methylbenzylamine (MBA) and 1-methyl-3-phenylpropylamine (MPPA) were separated from isopropyl amine (IPA). COSMO-RS was employed to screen over 200 organic mixtures, identifying twelve mixtures based on trioctylphosphine oxide (TOPO), lidocaine, and menthol as solvent candidates, due to their hydrophobicity. These mixtures were analysed for critical solvent properties including density, viscosity, hydrophobicity, and hydrogen bonding interactions. ME tests showed TOPO-thymol had the highest solvent residual and selectivity. Moreover, TOPO-thymol demonstrated solute fluxes of 9.0±3.0 g/(m^2 h) for MBA, 16.5±5.4 g/(m^2 h) for MPPA, and 0.7±0.3 g/(m^2 h) for IPA, with selectivity values of 12.4±0.8 for MBA/IPA and 22.8±1.4 for MPPA/IPA. Compared to undecane, which had lower selectivity values of 6.9±0.8 for MBA/IPA and 10.1±1.3 for MPPA/IPA, TOPO-thymol showed superior selectivity, indicating its promise as an extractant for ME applications.

Keywords Aromatic amines; Membrane extraction; COSMO-RS; Supported liquid membranes; TOPO-based solvents

1. Introduction

Chiral amines are a class of compounds, which have emerged as pivotal building blocks and intermediates for the pharmaceutical industry. Over 40% of all pharmaceutical products employ chiral amines during their production. Additionally, these compounds are used as resolving agents, precursors, and chiral auxiliaries for the synthesis of highly enantiopure organic molecules [1,2]. Especially, primary chiral amines are highly desirable in this domain, as they allow for a high degree of manipulation of the amine group [3]. One of the main challenges of chiral amines is their synthesis, which can be done chemically or biochemically. Although the chemical method is preferred due to its stability under harsh process conditions and well-known chemistry, costly and highly toxic transition metals are used as a catalyst [4]. On the other hand, the biochemical route provides an environmentally friendly alternative, as it uses enzymes as a biocatalyst [3,5]. The main advantage of using enzymes is their selectivity relative to the substrate, *i.e.*, they can differentiate between enantiomers in a racemic mixture. Furthermore, only mild process conditions are needed, *e.g.*, room temperature, neutral pH, and aqueous media [6,7].

Various enzymes have already been used for this route, such as lipases, imine reductases (IRED), amine dehydrogenases (AmDH), monoamine oxidases (MAO), and transaminases (TA). These different classes are presented in Fig. 1. Lipases, belonging to the hydrolase family, catalyse the formation and cleavage of amides and esters, with Bayer developing a lipase-based kinetic resolution process for producing chiral amines already in the mid-1990s. BASF also began industrial production of specific chiral amines using a lipase-catalysed approach. Imine reductases (IREDs) can enantio-selectively reduce imines to their corresponding amines using NADPH. Amine dehydrogenases (AmDHs) catalyse the reductive amination of ketones using NADH, whereas amine oxidases, a subgroup of oxidoreductases, facilitate redox reactions. Specifically, monoamine oxidases (MOAs) oxidise amines to imines while concurrently reducing O_2 to H_2O_2. Last, transaminases (TAs) can reversibly transfer amino groups from an amine donor to a ketone or aldehyde. Among the various enzyme possibilities, TAs offer distinct advantages in amine synthesis, due to their broad substrate range, outstanding enantioselectivity, high turnover rates, and the absence of a requirement for cofactor regeneration [1,8]. Various studies can be consulted for more details on the use of TAs for chiral amine synthesis [1,9–13].

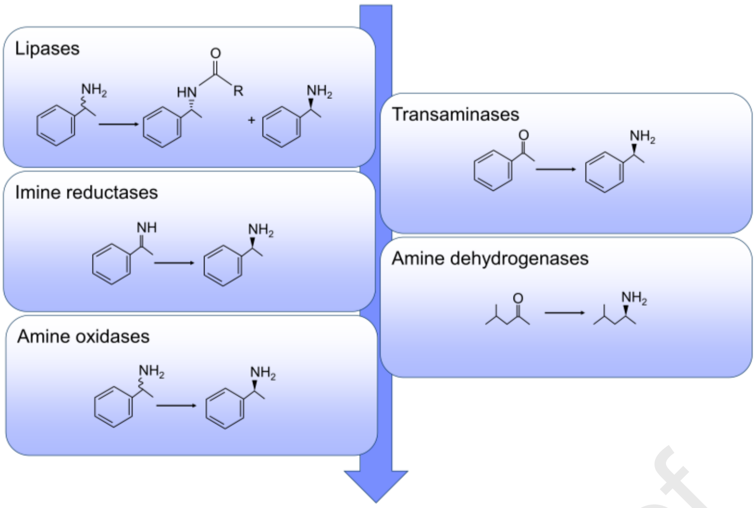

Fig. 1. Different enzyme classes for the enantioselective synthesis of chiral amines, adapted from Ghislieri et al. [7].

However, enzymes tend to be less stable in large-scale operations compared to the chemical synthesis [14]. Additionally, a significant drawback of using enzymes is the unfavourable thermodynamic equilibrium, which can lead to product inhibition [15]. To solve this issue, *in situ* product removal (ISPR) can be used to shift the equilibrium to the product side. The ISPR strategy can be performed using various technologies, including liquid-liquid extraction, but most techniques suffer from low solvent selectivity, high production costs, and a high environmental impact [16,17]. For a comprehensive overview of alternative ISPR and separation methods, the reader is referred to our previous review [18], along with the work of Tufvesson et al. [12] and Madsen et al. [19]. One prospective method for accomplishing ISPR is the use of supported liquid membranes (SLMs). An SLM is a three-phase system in which a liquid membrane phase is held inside of a microporous film by capillary forces. Usually, the membrane phase is an organic solvent, which separates two aqueous phases. The solutes can pass from the donor to the acceptor phase by diffusion through the membrane, due to a concentration, pressure, or electrical potential gradient. SLMs show many advantages compared to traditional extraction methods, such as low energy consumption, high selectivity, low separation cost, simplicity of operation, and low solvent usage. However, the main disadvantage of this technique is its impaired long-term stability and difficult solvent selection [20–22]. The solvent choice for SLMs becomes even more complex given the broad range of options that can serve as the membrane phase, including volatile organic solvents, ionic liquids (ILs), deep eutectic solvents (DESs), and solvent mixtures.

Deep eutectic solvents (DESs) are particularly intriguing for various extraction applications. According to Martins et al. [23], a DES is defined as “a mixture of pure compounds for which the eutectic point temperature is below that of an ideal liquid mixture”. In these mixtures, one compound serves as a hydrogen bond donor (HBD) and the other as a hydrogen bond acceptor (HBA), resulting in a eutectic mixture with a depressed melting point. This reduction in melting point is generally attributed to charge delocalisation caused by hydrogen bond interactions, as well as steric effects and ionic interactions, if an anion/cation pair is used. The stronger the hydrogen bonds compared to those in the precursor compounds, the more significant is the melting point reduction. DESs typically have a low production cost, simple preparation methods, and in general a high biodegradability and low toxicity [23,24]. Due to these characteristics, DESs are viable alternatives to conventional organic solvents and even alternative solvents, such as ionic liquids [25–27]. SLM applications using DESs have already been studied for gas separations [28–30], the separation of olefins [31–33], and the extraction of organics from aqueous solutions [34–36].

However, the extensive variety of hydrogen bond donors and acceptors still complicates the solvent selection process. To simplify the solvent choice, COSMO-RS can be used as a fast and effective tool to predict thermophysical and thermodynamical properties of fluids and fluid mixtures, without the need for experimental data. The strength of COSMO-RS lies in its ability to quickly compute chemical potentials and activity coefficients for compounds in liquid mixtures, making it a viable alternative to conventional group contribution methods (GCMs). When combined with a solvent database, COSMO-RS enables highly efficient and rapid thermodynamic calculations, including large-scale screening of solvents. For a more in-depth discussion of the COSMO and COSMO-RS methodology, the reader is referred to the works of Klamt [37–41] and others [42–44]. COSMO-RS has already been used in predicting various industrial processes, such as denitrification, desulfurisation, and the separation of aliphatic-aromatic mixtures. Additionally, several studies have used COSMO-RS for the facilitated screening of DESs in applications including antioxidant extraction [45], oil extraction from plant seeds [46], fucoxanthin extraction [47], and extraction of benzene from organic mixtures [48].

In this study, the use of supported liquid membranes (SLMs) was explored for the separation of aromatic amines. Specifically, the product amines α-methylbenzylamine (MBA) and 1-methyl-3-phenylpropylamine (MPPA) were separated from the donor amine isopropyl amine (IPA). Initially, COSMO-RS was employed to rapidly screen over 200 organic mixtures to evaluate their affinity and hydrophobicity. Subsequently, various organic mixtures were prepared by combining trioctylphosphine oxide (TOPO), lidocaine, and menthol with various HBDs, including carboxylic acids and thymol. TOPO is a conventional HBA for deep eutectic solvents (DESs), as evidenced by its frequent use in the literature [49–52]. The properties of the obtained mixtures, including density, viscosity, and hydrogen bond interactions, were then characterised. Finally, the stability of the prepared mixtures was tested, and the extraction performance and selectivity were evaluated for the most stable mixtures in conventional SLM tests.

2. Material and methods

2.1 Chemicals and membranes

The chemicals, as listed in Table 1, were used for the experimental work in this study. The molecular structures of these compounds can be found in Fig. S1 in the Supplementary Material. A polytetrafluoroethylene (PTFE) membrane with a pore size of 50 nm, kindly provided by Donaldson, was used as the support material in the membrane extraction tests.

Table 1. Overview of the used chemicals in this work.

Compound	Acronym	Purity, %	Supplier
Octanoic acid	C8 acid	98	Alfa Aesar
Nonanoic acid	C9 acid	97	Thermo Fisher Scientific
Decanoic acid	C10 acid	99	Acros Organics
Dodecanoic acid	C12 acid	98	Sigma Aldrich
Oleic acid	Ole acid	T.R.	Carl Roth
Thymol	Thy	> 99	VWR
Trioctylphosphine oxide	TOPO	99	Sigma Aldrich
Lidocaine	Lid	> 99	TCI Europe
Menthol	Men	≥ 95	Sigma Aldrich
Sodium carbonate	Na_2CO_2	≥ 99.9	Merck Life
Sodium bicarbonate	$NaHCO_3$	A.R.	Fisher Scientific
Sodium dihydrogen phosphate	NaH_2PO_4	≥ 98	VWR
Phosphoric acid	H_3PO_4	85	VWR
Sodium hydroxide	NaOH	≥ 98.5	VWR
α-Methylbenzylamine	MBA	98	Merck Life
1-Methyl-3-phenylpropylamine	MPPA	98	Sigma Aldrich
Isopropyl amine	IPA	≥ 99.5	Sigma Aldrich

2.2 Preparation of organic solvent mixtures

The extractant preparation is notably simple as the process involves direct mixing of the HBA and the HBD in a specific molar ratio. The molar ratio was chosen based on literature, where an HBA/HBD molar ratio of 1:2 is commonly used [53,54]. If this ratio did not yield a liquid mixture, then a 1:1 molar ratio was used. Both the HBA and HBD were weighed and added to a bottle, after which the mixture was added to a water bath and heated to 80 °C under continuous stirring. The mixture was allowed to remain on the hotplate, until it became homogeneous and transparent, for a maximum duration of five hours [36,55,56]. All the liquid mixtures prepared in this work are given in Table 2.

Table 2. Overview of the prepared organic mixtures with their HBA and HBD.

HBA	HBD	Molar ratio
Lid	C8 acid	1:2
Lid	C9 acid	1:2
Lid	C10 acid	1:2
Men	C8 acid	1:2
Men	C9 acid	1:2
Men	C10 acid	1:2
TOPO	C8 acid	1:2
TOPO	C9 acid	1:2
TOPO	C10 acid	1:2
TOPO	C12 acid	1:1
TOPO	Ole acid	1:2
TOPO	Thy	1:2

2.3 Experimental analysis of critical solvent parameters

The density and viscosity of the considered mixtures were measured at 25 °C with a Lovis 2000 ME rolling-ball type viscometer (Anton Paar). This was accomplished using three capillaries of distinct sizes, namely 1.59, 1.8, and 2.5 mm in diameter. A maximum coefficient of variation of 1% and an angle of 70° were used during the whole procedure. The apparatus was cleaned with acetone and water between each measurement.

To analyse the hydrogen bonding interactions and their impact on the mixture properties, FTIR analysis using a Nicolet iN10 Infrared Microscope was conducted on both the mixtures and their constituents. First, the equipment was cooled down using liquid nitrogen. For liquid samples, a droplet of the compound or mixture was placed on a rectangular crystal plate, which was spread uniformly on the plate until a thin layer was obtained. This plate was then positioned horizontally above the light beam of the device. The camera was adjusted to obtain a clear image of both the sample and the background. For solid samples, a small amount of the compound was first ground with potassium bromide using a mortar and pestle. After grinding, the powder was compacted into a small pellet using a circular mould, by applying 10 bar of pressure, to ensure that light can pass through effectively. The pellet was then added to the sample plate. The software Omnic-Picta was used for data analysis.

2.4 Membrane impregnation

To perform the membrane impregnation, the membrane and filter paper were cut into circles with a diameter of approximately 46 mm. The membrane was weighed using an analytical scale. Next, the filter paper was positioned on the Büchner filter, and the membrane was placed on top of the filter. After ensuring the membrane covered the entire surface, the vacuum pump was turned on. Then, 1 to 2 mL of the considered mixture was pipetted on the membrane and spread with a spatula until the membrane surface was covered completely. To ensure a complete impregnation, the vacuum pump was left running for 45 minutes. After the designated time, the vacuum pump was turned off, the excess of the mixture was wiped off with a paper towel and the membrane was weighed again using an analytical scale. To assess the membrane affinity for the mixture, the impregnation efficiency was defined as the liquid mixture uptake in the membrane pores divided by the membrane surface area [57]:

$$\text{Impregnation efficiency} \left(\frac{\mathrm{g}}{\mathrm{m}^2}\right) = \frac{m_{\mathrm{wet}} - m_{\mathrm{dry}}}{A} \quad (1)$$

in which m_{dry} (g) is the weight of the dry membrane before impregnation, m_{wet} (g) the weight of the membrane after impregnation, and A (m²) the membrane surface area. To assess the membrane stability, the weight of the membrane was recorded before and after the extraction test to determine the solvent loss. The solvent residual after the test was calculated as follows [57]:

$$\text{Solvent residual } (\%) = \frac{m_{\mathrm{after}} - m_{\mathrm{dry}}}{m_{\mathrm{wet}} - m_{\mathrm{dry}}} \cdot 100\% \quad (2)$$

in which m_{after} (g) is the weight of the membrane after the experiment.

2.5 Membrane extraction experiments

For the extraction tests, a feed and a strip buffer solution were prepared at a pH of 10 and 3, respectively. For the feed solution, 500 mL of Milli-Q water was added to a beaker. Then, 3.79 g of Na_2CO_3 and 5.38 g of $NaHCO_3$ were weighed and added to the beaker. The solution was mixed until the compounds were fully dissolved. Then, 250 mg of each amine, namely, α-methylbenzylamine (MBA), 1-methyl-3-phenylpropylamine (MPPA) and isopropyl amine (IPA), were added to the solution. Similarly, for the strip solution, 500 mL of Milli-Q water was added to a beaker, after which 10.49 g of NaH_2PO_4 was weighed and added. The solution was mixed until complete dissolution was obtained. Next, 862 µL of an 85% (w/w) solution of H_3PO_4 was added [58].

The setup for the membrane extraction is shown in Fig. 2. Two gear pumps were used to circulate the feed and strip solution counter-currently at a flow rate of 10 L/h. A membrane contactor with a spiral pattern was used to maximise the surface contact between the two phases. The pressures at the in- and outlets of the membrane contactor were recorded, as well as the flow rates and temperatures of the feed and strip solution. Samples of the feed and strip solution were collected at the start of the experiment and after 1, 3, 6 and 24 hours. The concentration of MBA and MPPA was analysed using HPLC-UVVIS (Shimadzu Prominence-I LC-2030C 3D) with acetonitrile and 0.1 v% H_3PO_4 as the mobile phases, while the IPA concentration was determined using headspace GC-FID (Autosystem XL, PerkinElmer) with helium as the mobile phase. An Rtx-5 Amine (30 m, 0.25 mm, 0.50 µm) was used as the column. Additionally, 200 μL of a 25% NaOH solution was added to the feed and strip sample to achieve a sufficiently high pH in the solution, as IPA can only volatilise at an elevated pH [57,58].

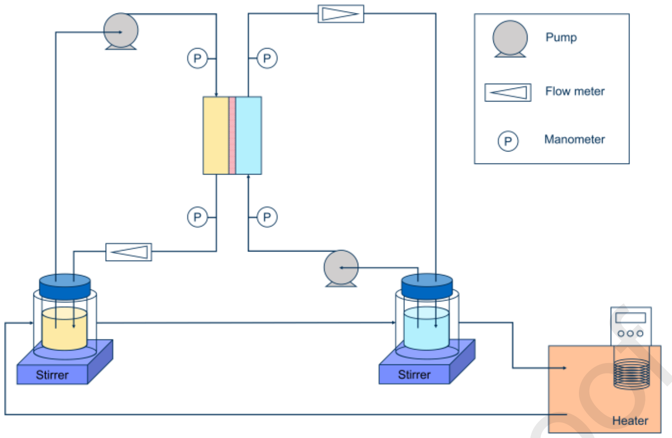

Fig. 2. Schematic diagram of the used membrane extraction setup, adapted from Van Eygen et al. [58].

The fluxes of solute i (MBA, MPPA, or IPA) for the ME experiments were determined as follows:

$$J_i\left(\frac{\mathrm{g}}{\mathrm{m^2h}}\right) = \frac{C_f(t_1)-C_f(t_2)}{t_2-t_1}\frac{V}{A_{\mathrm{eff}}} \quad (3)$$

in which $C_f(t)$ is the feed concentration of the solute (g/L) at time t (h), V the feed volume (L), and A_{eff} the effective membrane surface area (m²). The membrane surface area was equal to 0.000561 m². The feed volume is assumed to be constant at 250 mL over 24 hours, as the loss due to sampling is considered negligible. The times t_1 and t_2 are time points in between which the flux has stabilised (see Fig. S2). The overall process selectivity S_{ij} of solute i over solute j was determined by calculating the flux ratio of those compounds:

$$S_{ij}(/) = \frac{J_i}{J_j} \quad (4)$$

in which J_i is the flux of solute i (g/(m²h)). The recovery of solute i could be defined as:

$$R_i(\%) = \frac{C_f(t_1)-C_f(t_2)}{C_f(t_1)} \quad (5)$$

2.6 COSMO-RS simulations

The quantum calculations were performed using the density functional theory (DFT) with a resolution identity (RI) approximation in the TmoleX v. 4.5 software package. Furthermore, to check if an electronic energy minimum was achieved, vibrational frequency calculations were performed. To obtain the optimised geometries of the HBAs and HBDs, a triple zeta valence polarised basis set (def-TZVP), the

Becke-Perdew (BP-86) functional level of theory, and the COSMO-solvation model were used. These optimised geometries were stored as COSMO files. The presence of an optimised energy state was then confirmed using the vibrational frequency calculations. Finally, the thermodynamic properties of the considered mixtures were predicted using the generated COSMO files as an input in COSMOthermX. Within COSMO-RS, the mixtures are represented according to the molar composition of their constituents [59–61]. For a more in-depth description of the COSMO-RS model, Section SD-3 in the Supplementary Material can be consulted.

3. Results and Discussion

3.1 COSMO-RS screening

COSMO-RS was used for a primary screening of various organic solvent mixtures according to their selectivity towards the target amines MBA and MPPA over the donor amine IPA. The selectivity is directly affected by the activity coefficient at infinite dilution of the solutes, a key factor that determines their preferential interaction with a specific phase, either the aqueous or organic phase. The selectivity can be defined as the ratio of the partition coefficients of the target amine (either MBA or MPPA) over the donor amine IPA [48,58].

$$S_{\mathrm{AB}} = \frac{K_{\mathrm{A}}}{K_{\mathrm{B}}} = \frac{\left(\frac{\gamma_{\mathrm{A}}^{\mathrm{I}}}{\gamma_{\mathrm{A}}^{\mathrm{II}}}\right)}{\left(\frac{\gamma_{\mathrm{B}}^{\mathrm{I}}}{\gamma_{\mathrm{B}}^{\mathrm{II}}}\right)} \tag{6}$$

in which γ represents the activity coefficient at infinite dilution. The subscripts A and B denote the target amines and the donor amine, respectively, and the superscripts I and II represent the aqueous and organic phase, respectively [58].

For the COSMO-RS simulations, thirteen organic acids, four terpenes, six alcohols, two parabens, four phenols, choline chloride (ChCl), and TOPO were selected as the mixture constituents. The considered compounds and their abbreviations are given in Table S1. The separation into HBAs and HBDs is based on the capacity of a specific compound to function primarily as a donor or an acceptor in hydrogen bond interactions. The hydrogen bond donor and acceptor moments were calculated for each compound using COSMO-RS. The results can be seen in **Fig. *3***a. Camphor, TOPO, and choline chloride all have a very low HBD moment, indicating their HBA character. Menthol and lidocaine and all the considered alcohols are better suited as HBAs, as their HBD/HBA < 1. On the other hand, thymol and all the acids, phenols, and parabens are better HBDs, as their HBD/HBA > 1. Next to their HBA and HBD moments, the dipole moment, which is a measure for the polarity of the molecule, was calculated using COSMO-RS. From **Fig. *3***b, all the acids and terpenes show a similar polarity. Only choline chloride shows a much larger dipole moment due to its charged character.

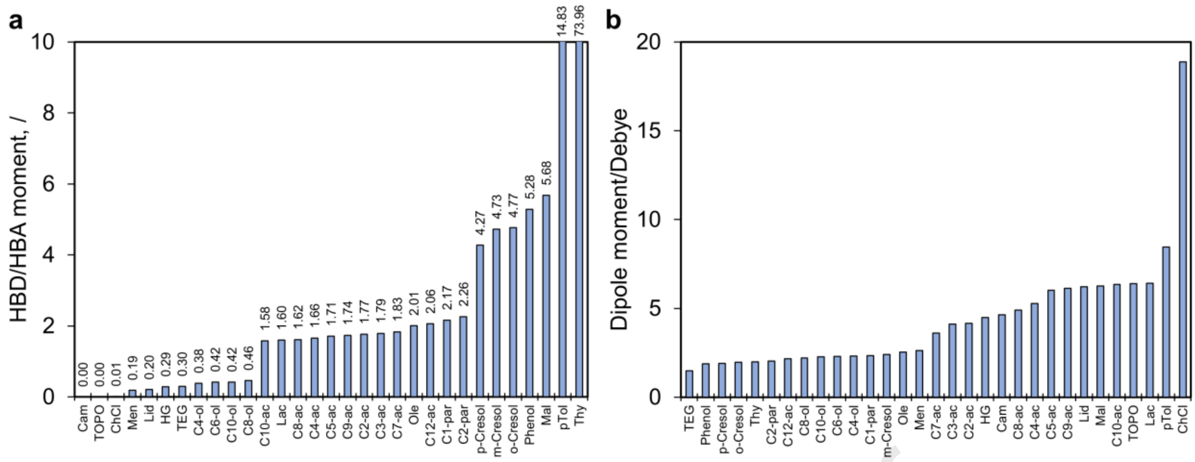

Fig. 3. Simulated results of (a) the ratio of the HBA and HBD moment of various compounds, and (b) the dipole moment of various compounds, obtained by COSMO-RS. The abbreviations of the compounds are given in Section SD-4 in the Supplementary Material.

The simulated MBA/IPA and MPPA/IPA selectivities are given in Fig. 4 for various organic mixtures. All the simulated mixtures display a preferential selectivity towards the target amines MBA and MPPA, compared to the donor amine IPA. This can be attributed to the significantly lower activity coefficient of IPA in the aqueous phase ($\gamma_{\mathrm{IPA}}^{\infty}$ = 4.9), whereas MBA and MPPA show a much lower affinity for this phase ($\gamma_{\mathrm{MBA}}^{\infty}$ = 76.2 and $\gamma_{\mathrm{MPPA}}^{\infty}$ = 240.1). Moreover, all mixtures demonstrate a higher MPPA/IPA selectivity than MBA/IPA selectivity. The HBA choice impacts the overall selectivity more than the HBD. For MBA, the choice is less critical as the selectivity ranges between 2 and 7. However, for MPPA, three HBAs – camphor, lidocaine, and TOPO – demonstrate a significantly higher selectivity. Alcohols show a lower selectivity, which decreases with a longer alkyl side chain length. These compounds have a very high HBA moment (see **Fig. *3***a), indicating that strong hydrogen bonds can be formed. The choline-chloride based mixtures do not exhibit a high MPPA/IPA selectivity, likely due to their hydrophilic nature, which is indicated by their higher polarity than water, as noted by Cicci et al. [62].

Based on the simulations, the choice of the HBD is less crucial. From Fig. 4, both the phenols and parabens show very similar selectivity values when used as HBDs. However, these compounds were omitted from the selection due to their inherent toxicity [63,64]. Carboxylic acids and thymol seem to provide satisfactory selectivity values as the HBD. For the alcohols, similar to the acids, an increase in the alkyl side chain length leads to a decrease in the selectivity. More complex alcohols with shorter alkyl chains, such as tetraethylene glycol and hexylene glycol, show enhanced selectivity. The presence of shorter alkyl chains, which enable the formation of dominating hydrogen bond interactions, leads to a better selectivity. For phenyl alcohol derivatives (PhAs), it was also found that with an increasing chain length, the contribution of dispersive forces compared to hydrogen bonds becomes more significant to the association degree. Hence, PhAs associate better if they contain longer alkyl chains [65]. The increase in the alkyl chain leads to better association between the HBA and HBD, making it more difficult for the bulkier compounds MBA and MPPA to interact with the mixture, as opposed to the smaller IPA molecule, explaining their reduced selectivity. This contrasts with [N(Tf)$_2$]-based ionic liquids (ILs), where an increase in the cation alkyl chain length leads to a higher selectivity due to enhanced hydrophobicity [58,66]. It should be noted that this effect cannot be generalised to all ionic liquids, as the effect of the cation alkyl chain length on the ionic liquid selectivity is dependent on the used anion type [67].

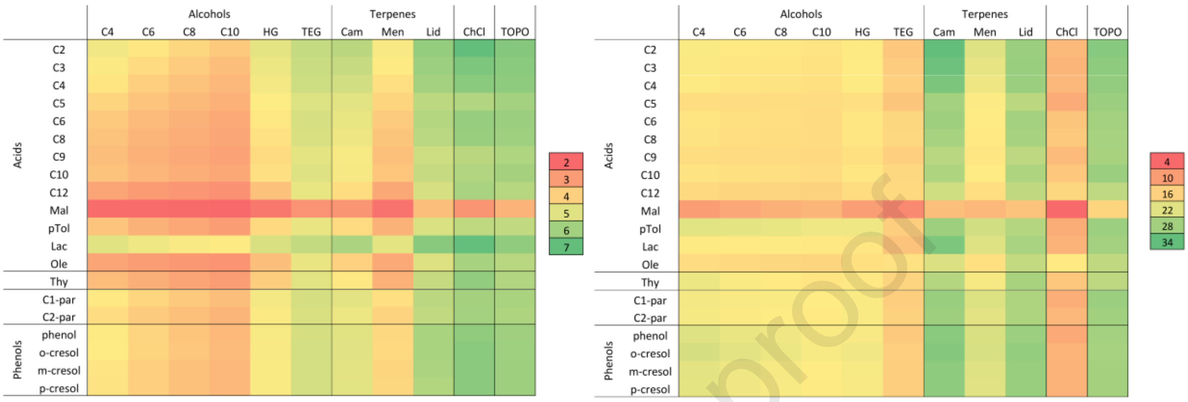

Fig. 4. The organic mixture selectivity for (left) MBA/IPA, and (right) MPPA/IPA for various equimolar mixtures at 25 °C, obtained by COSMO-RS simulations. The abbreviations are given in Section SD-4 in the Supplementary Material.

Based on Fig. 4, twelve organic mixtures were selected to experimentally evaluate the effect of the mixture composition on the final extraction performance. Five organic acids (*i.e.*, octanoic, nonanoic, decanoic, dodecanoic acid, and oleic acid) and the terpene thymol were selected as the HBDs, while lidocaine, menthol, and TOPO were selected as the HBAs, as listed in Table 2. Choline chloride was removed from the HBA candidates, as ChCl-based mixtures exhibit an impaired MPPA/IPA selectivity, as can be seen in Fig. 4. Furthermore, lidocaine, menthol, and TOPO have already been used successfully for the preparation of hydrophobic mixtures for extraction applications [49,54].

In a mixture, the affinity of a compound towards the other compounds can be analysed by their σ-profile and -potential. The σ-profile provides a histogram of the charge density distribution over the surface of the molecule, whilst the σ-potential gives a measure of the affinity of a compound in a mixture towards the others. If the screening charge density σ is in the range [-0.0085; 0.0085] eÅ^{-2}, then the molecular surface is too non-polar to participate in hydrogen bonding interactions. For σ < -0.0085 eÅ^{-2}, the molecular surface may interact as a hydrogen bond donor, and for σ > 0.0085 eÅ^{-2}, as a hydrogen bond acceptor [47]. The σ-profiles of the considered solutes are given in Section SD-5 in the Supplementary Material. The σ-profiles of MBA, MPPA, and IPA are all mostly located in the non-polar region, but the peaks of MBA and MPPA are larger, indicating that they are more non-polar than IPA. Additionally, all three amines have a small peak at σ < -0.0085 eÅ^{-2}, indicating their ability to act as a HBD. Therefore, solvents that are predominantly non-polar and that can act as a HBA should show a higher selectivity towards the target amines MBA and MPPA. The σ-profiles of the considered mixture compounds are given in Section SD-6 in the Supplementary Material. All the acids (namely, octanoic, nonanoic, decanoic, dodecanoic, and oleic acid) have their main peaks in the non-polar region, next to a small peak in the HBA region, while thymol is primarily non-polar. Among the HBAs, TOPO exhibits the largest peak in the non-polar region, making it a suitable candidate for extracting the target amines. In contrast, both lidocaine and menthol display lower peaks, although they are also primarily in the non-polar region.

3.2 Extractant characterisation

3.2.1 Density characterisation

The density values of the prepared mixtures are given in Fig. 5a and b for various hydrogen bond donors and acceptors, respectively. All the considered mixtures exhibit densities lower than 1 g/mL and specifically in the range between 0.88 and 0.97 g/mL. Hydrophobic DESs prepared with neutral compounds generally have densities lower than water, which aids in the segregation of the aqueous and organic phase in extractive applications [68]. This contrasts with most hydrophilic DESs, which generally have a density higher than water (around 1.15 g/mL) [54].

The mixture density is strongly correlated with the individual density of the mixture constituents. For example, the lidocaine-based mixtures have a much higher density, as lidocaine itself has a higher density of 0.979 g/mL compared to the other compounds (see Table S2 in the Supplementary Material). Moreover, the density decreases for an increase in the alkyl chain length of the carboxylic acids (see Fig. 5b) for all tested HBAs. This was also observed by Nunes et al. [69] for menthol-based DESs. Data from this work align with the literature (see Table S3 in the Supplementary Material).

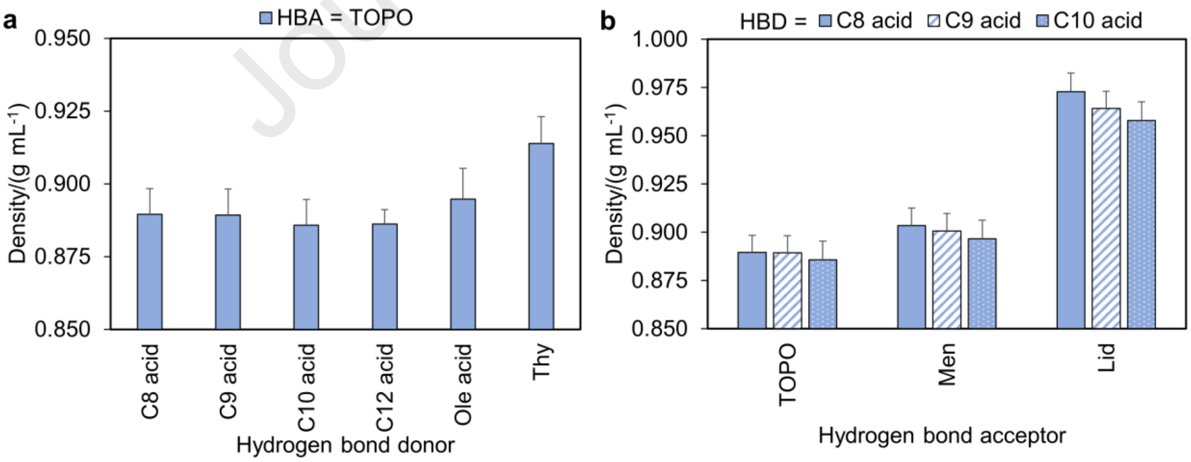

Fig. 5. Experimental densities of organic mixtures: (a) different HBDs combined with TOPO as the HBA; (b) different HBAs combined with carboxylic acids as the HBD. All mixtures were prepared using a 1:2 molar ratio of HBA to HBD. Abbreviations are listed in Table 1.

3.2.2 Viscosity characterisation

The viscosity values of the prepared mixtures are given in Fig. 6a and b for various hydrogen bond donors and acceptors, respectively. The viscosities of all mixtures, except for the lidocaine-based mixtures, are lower than 100 cP. This contrasts with hydrophilic DESs, which generally have a relatively high viscosity limiting mass transfer. Similar to the density values, the use of neutral compounds leads to solutions of lower viscosity [68]. Generally, longer alkyl chains imply a greater potential for Van der Waals interactions, leading to a higher viscosity [70,71]. For example, the TOPO-based mixtures with octanoic, nonanoic, and decanoic acid show a similar viscosity around 31 cP, while the mixture with dodecanoic acid has a larger viscosity of 45 cP. The use of lidocaine as the HBA leads to a significantly higher viscosity, compared to TOPO and menthol.

As previously mentioned, highly viscous mixtures are desired, which leads to a higher SLM stability [58,72]. Although, it should be noted that too viscous mixtures can be problematic for industrial process application, as it requires more time for compounds to diffuse through the membrane, leading to increased costs. Hence, the ideal viscosity for mixtures used in industrial processes is below 100 cP [73]. Data from this work align with the literature (see Table S3 in the Supplementary Material), although larger viscosity variations can be observed, potentially due to differences in water content, as no drying stage was used prior to analysis in this work.

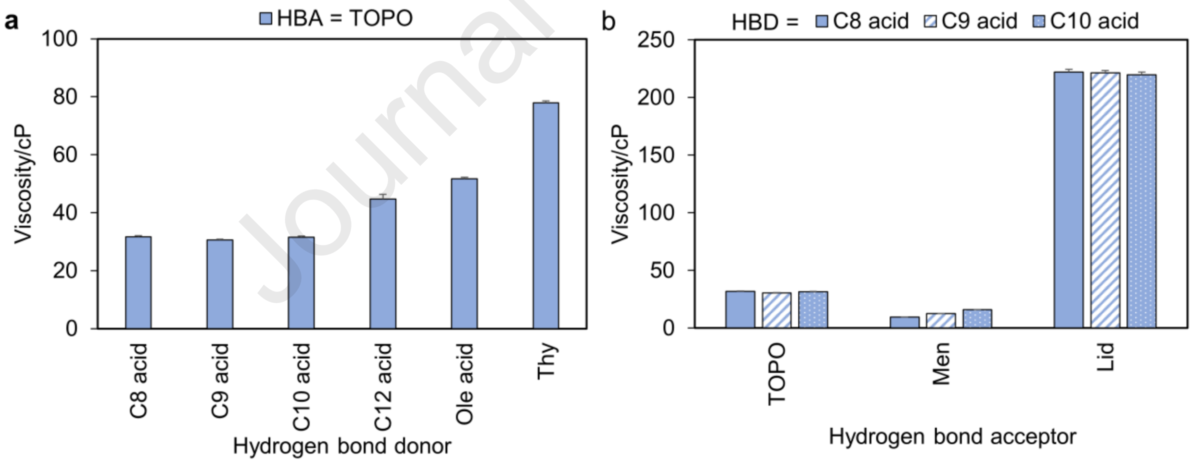

Fig. 6. Experimental viscosities of organic mixtures: (a) different HBDs combined with TOPO as the HBA; (b) different HBAs combined with carboxylic acids as the HBD. All mixtures were prepared using a 1:2 molar ratio of HBA to HBD. Abbreviations are listed in Table 1.

3.2.3 Hydrophobicity and intermolecular interactions

The presence of hydrogen bonds formed between the two constituents of a mixture can be discerned in an FTIR spectrum through shifts in the position of their transmittance peaks, indicating transitions between spectra. This technique has already been used in various studies in the literature for the analysis of hydrogen bonds in polymer blends [74,75], gels [76], and alcohol-ester mixtures [77].

According to Cao et al. [54], the strength of hydrogen bonds in photo-excited fluorescent dyes can be inferred from red- and blue-shifts. A redshift occurs when an X-H bond (with X being more electronegative) elongates, allowing it to interact with Y (an element with available electron pairs). This causes a shift of IR absorption peaks to lower wavelengths, indicating stronger hydrogen bonding. In contrast, a blueshift reflects weaker hydrogen bonds, shortening the X-H bond and shifting absorption peaks to higher wavelengths [78,79].

The FTIR spectra of the different TOPO-based mixtures are given in Fig. S6 and for the lidocaine- and menthol-based mixtures in Fig. S7. Theoretically, the P=O bond of TOPO functions as the sole HBA site, which can interact with the hydroxide group of carboxylic acids or of thymol. The FTIR spectra of the carboxylic acids show broad peaks around 2400-3200 cm^{-1} (see Fig. S6a-d), which can be attributed to O-H stretching of a carboxylic acid. Additionally, both TOPO and the carboxylic acids show a broad peak around 3400-3600 cm^{-1} (see Fig. S6a-d), possibly due to water absorption [79]. Interestingly, the FTIR spectrum of the TOPO-based mixtures lack these broad peaks, indicating the formation of stronger hydrogen bonds between TOPO and the carboxylic acid and a lower water absorption. On the other hand, for the lidocaine- and menthol-based mixtures, the broad peaks at 2400-3200 cm^{-1} are still present (see Fig. S7), except for lidocaine-octanoic acid. Notably, for TOPO-thymol, a clear redshift can be observed for the O-H stretching peak from 3450 to 3200 cm^{-1}, indicating strong hydrogen bonding interactions.

COSMO-RS simulations can calculate the interaction energies for the considered mixtures. Various studies have already shown that generally COSMO-RS can predict well the excess enthalpies of various solvent types, including ionic liquids and DESs [80,81]. This excess enthalpy of mixing or interaction (H_{int}), calculated as a temperature derivative of the Gibbs free energy, enables a more detailed analysis of the contributions from different interaction types, which are represented through COSMO-RS as follows [80,82]:

$$H_{\mathrm{int}} = H_{\mathrm{MF}} + H_{\mathrm{HB}} + H_{\mathrm{VDW}} \tag{10}$$

In which H_{MF} is the enthalpic penalty accounting for steric hindrance and charge misalignment, and H_{HB} and H_{VDW} are the contributions from hydrogen bonding and van der Waals interactions [80]. Fig. 7a and b present the total mean interaction energy of the HBA and HBD for different hydrogen bond donors and acceptors, respectively. Fig. 7a reveals that the hydrogen bond acceptor TOPO exhibits a higher interaction energy than the HBDs. Additionally, it shows that as the alkyl chain length of the carboxylic acid increases from eight to twelve carbon atoms, the interaction energy from the acid increases. Fig. 7b demonstrates that TOPO has a significantly higher interaction energy compared to the other HBAs menthol and lidocaine, which is in line with the FTIR analysis. Again, an increase in the interaction energy of the acid is visible with a longer chain length. The contributions of the total interaction energy are provided in Section SD-8 of the Supplementary Material. It is evident that the van der Waals interactions (due to dispersion) are the primary contributors to the total mean interaction energy. Both the contributions due to hydrogen bonding and van der Waals interactions increase with a longer alkyl side chain of the carboxylic acid.

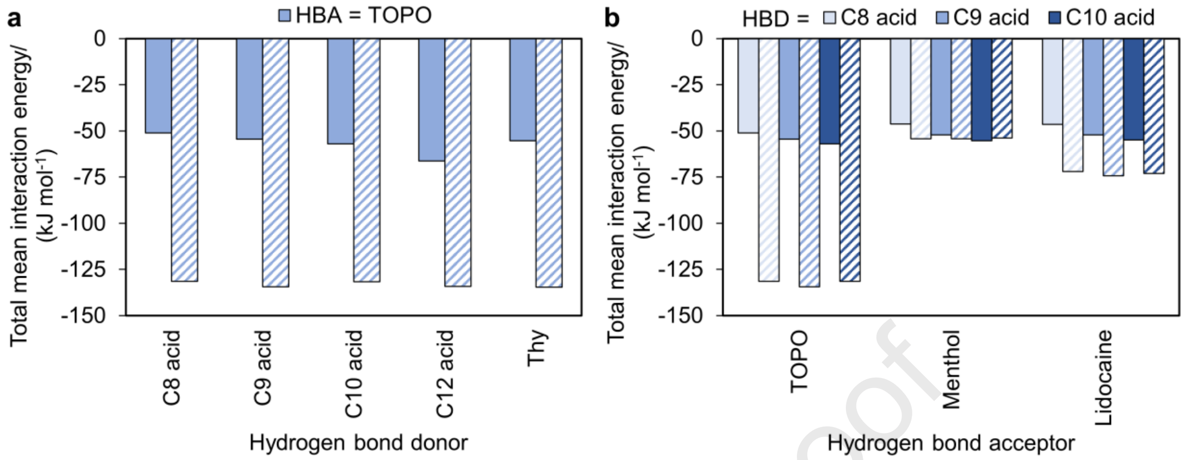

Fig. 7. COSMO-RS analysis of the total interaction energies of the HBD (represented by full bars) and HBA (represented by dashed bars) in organic mixtures: (a) different HBDs combined with TOPO as the HBA; (b) different HBAs combined with carboxylic acids as the HBD. All mixtures were prepared using a 1:2 molar ratio of HBA to HBD. Abbreviations are listed in Table 1.

3.3 SLM stability and extraction performance

3.3.1 Impregnation efficiency and SLM stability

A summary of the impregnation results and stability data after the tests can be found in Fig. 8a and b for the TOPO- and lidocaine-based mixtures, respectively. All the TOPO-based mixtures demonstrate a similar impregnation efficiency of around 40 to 50 g/m², as shown in Fig. 8a. This indicates that the PTFE membrane has a comparable affinity for all mixtures. For the lidocaine-based mixtures, a similar affinity was observed, except for lidocaine-octanoic acid, which showed an impregnation efficiency of approximately 150 g/m². This high value is likely an experimental artefact caused by layering of the liquid mixture on top of the membrane surface rather than filling of the pores. More importantly, all impregnated membranes experienced solvent loss after 24 hours. Notably, the lidocaine-based mixtures are less stable than the TOPO-based mixtures, with lidocaine-nonanoic acid retaining only 20% of the solvent. In contrast, the TOPO-based mixtures demonstrated improved stability up to 78.5% for TOPO-thymol. However, some variability in stability values was observed, indicating a non-negligible effect of the operating conditions on the overall membrane stability. The higher stability of TOPO-thymol could be attributed to its significantly higher viscosity (77.9 cP) compared to other TOPO-based mixtures, which range between 31.7 and 51.7 cP.

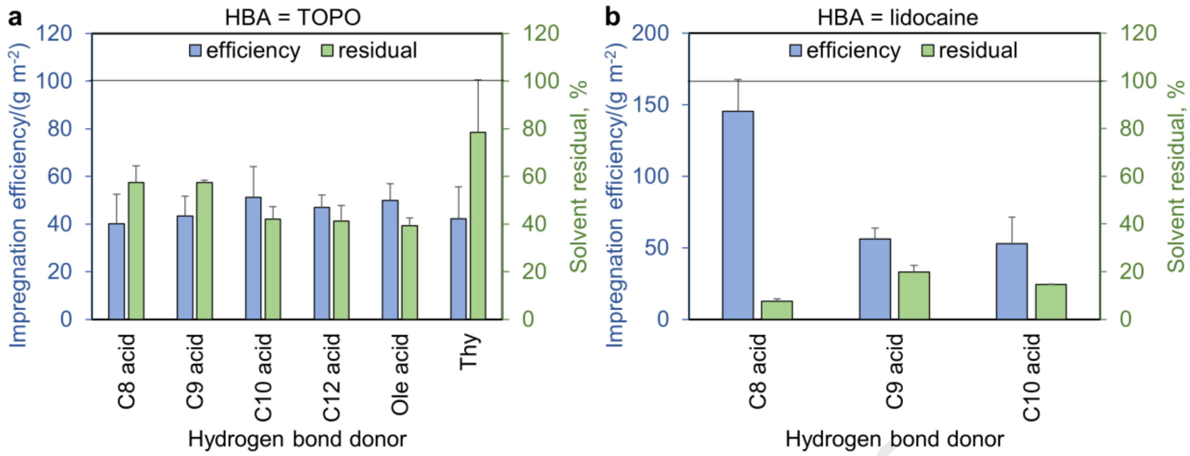

Fig. 8. Experimental results showing the impregnation efficiency of the PTFE membrane and solvent residuals following a ME test of 24 hours for organic mixtures containing various HBDs combined with (a) TOPO or (b) lidocaine as the HBA. All mixtures were prepared using a 1:2 molar ratio of HBA to HBD. Abbreviations are listed in Table 1.

Although the lidocaine-based mixtures have a significantly higher viscosity than the TOPO-based mixtures (see Fig. 6b), their SLM stability is compromised. Mjalli et al. [83] reported that when water is added to a DES phase, the water molecules can penetrate this phase and disrupt the strong hydrogen bonding interactions among the DES constituents. Additionally, Pandey et al. [84] found that the introduction of water enhances interspecies hydrogen bonding between the added water and the DES constituents. Florindo et al. [85] also stated that hydrogen bonds within DESs can be partially broken when brought into contact with water, after which the individual DES constituents can penetrate the aqueous phase according to their individual water solubility. The water solubility of the individual mixture constituents used in this work is detailed in Table S2.

Therefore, it is hypothesised that SLM stability depends on the interplay between the water miscibility of the liquid mixture and the strength of the intermolecular hydrogen bonding interactions among its constituents. For example, lidocaine-decanoic acid (2:1) has a water content of 20.6% after mixing with water, indicating that water can easily infiltrate this mixture [86]. Furthermore, the considered lidocaine-based DESs have a lower hydrogen bonding interaction energy compared to the TOPO-based DESs (see Fig. S8d), making them more susceptible to disruption by penetrating water molecules. Additionally, as shown in Fig. S6a-d, the FT-IR spectra of the TOPO-based mixtures lack the broad peaks around 3400-3600 cm^{-1}, while such peaks are still present in both lidocaine- and menthol-based mixtures (see Fig. S7), suggesting the formation of stronger hydrogen bonds in TOPO-based mixtures.

In summary, a high viscosity and low water miscibility of the final liquid mixture, along with a low water solubility of its individual components and strong hydrogen bonding between them, contribute to the formation of hydrophobic and stable organic mixtures. Among the tested systems, only the TOPO-thymol mixture demonstrated sufficient stability for amine extraction, with no volume exchange between the feed and strip buffer, and no changes in the pH of the buffers.

3.3.2 Extraction efficiency

The membrane extraction performance is given as a transmembrane flux of the considered solutes, namely MBA, MPPA, and IPA. The definition of this flux is given in Section 2.5 and the obtained fluxes and recoveries are given in Fig. 9. It can be observed that TOPO-thymol presents fluxes and recoveries which are much higher compared to the ionic liquid $[P_{6,6,6,14}][N(Tf)_2]$ for both MBA and MPPA. It should be mentioned that the mass balances for MBA and MPPA correspond almost perfectly, while no increase in the IPA concentration can be found in the strip solution. This can be due to multiple factors, such as a preference of IPA to remain in the membrane phase or volatilisation of IPA from the feed solution. As can be seen in Fig. 9a, MPPA shows a higher flux and recovery compared to MBA and IPA which can be linked to the COSMO-RS data, stating that all mixtures show a higher affinity towards MPPA, compared to MBA and IPA.

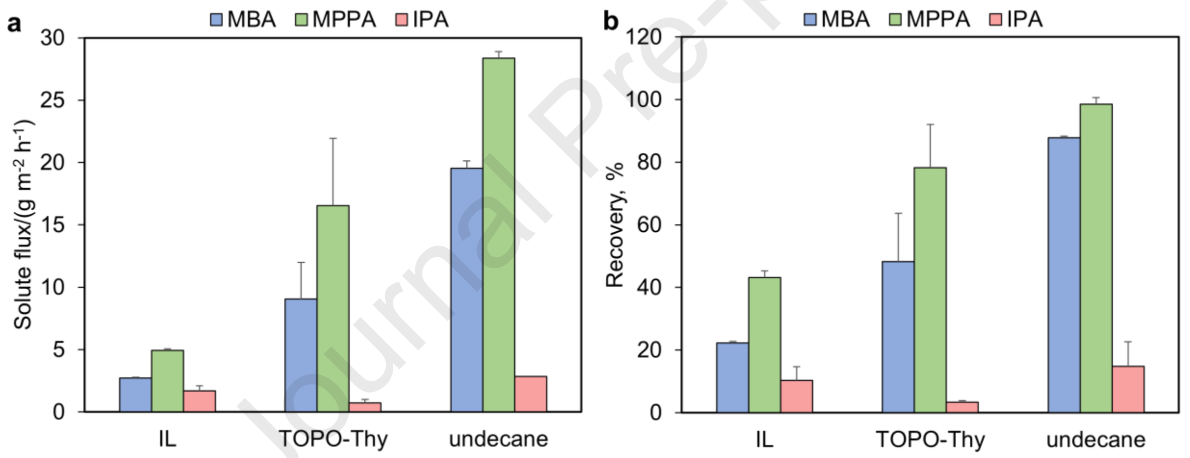

Fig. 9. Experimental results of (a) the solute fluxes, and (b) the recovery of the considered amines, through the supported liquid membrane wetted with TOPO-thymol compared to the benchmark solvents undecane and $[P_{6,6,6,14}][N(Tf)_2]$. The data of the benchmark solvents were obtained from Van Eygen et al. [58].

In addition to the overall flux, the selectivity is an important process parameter. The selectivity can be defined as the ratio of the MBA or MPPA flux to the IPA flux. As can be seen in Fig. *10*, the MPPA/IPA values are higher compared to the MBA/IPA for every extractant, implying a higher selectivity for MPPA. The overall selectivity of the target amines over the donor amine remains high, due to IPA having a low activity coefficient in the aqueous phase compared to the activity coefficient of the targeted amines, which indicates a preference for MBA and MPPA to transfer to the organic phase [58]. The mixture TOPO-thymol gives the highest selectivity for the target amines, with an MPPA/IPA selectivity twice as high as undecane. The high selectivity of TOPO-thymol, linked with its high solvent residual, indicates that this mixture is the best suited for the extraction process. Additionally, the reusability of TOPO-based DESs has already been investigated in various studies [87,88].

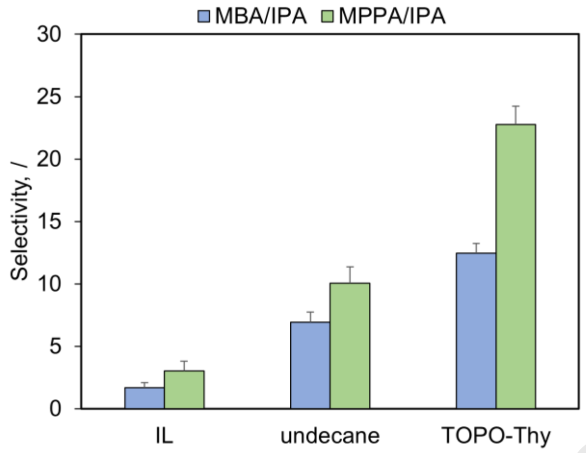

Fig. 10. Experimental results of the selectivity of the target amines MBA and MPPA over IPA through the supported liquid membrane wetted with TOPO-thymol compared to the benchmark solvents undecane and $[P_{6,6,6,14}][N(Tf)_2]$. The data of the benchmark solvents were obtained from Van Eygen et al. [58].

A comparison with previous studies is given in Table 3. Variations in fluxes can occur due to differing conditions, such as using a different extractant phase or feed concentration. However, the current study shows a significant improvement of the fluxes, compared to the literature data.

Table 3. Comparison of flux and feed concentration data for supported liquid membrane extraction of amines.

C_{MBA}/ (g/L)	J_{MBA}/ (g/(m^2/h))	C_{MPPA}/ (g/L)	J_{MPPA}/ (g/(m^2/h))	C_{IPA}/ (g/L)	J_{IPA}/ (g/(m^2/h))	Ref.
0.50	2.73	0.50	4.93	0.50	1.24	[57]
0.12	0.06	-	-	-	-	[89]
2.42	0.67	2.98	0.64	59.11	0.08	[90]
0.50	9.04	0.50	16.55	0.50	0.74	This study

4. Conclusions

In this study, various liquid mixtures were investigated as selective extractants for SLM extraction of aromatic amines. Initial screening of over 200 organic mixtures was performed using COSMO-RS simulations, which revealed that the molecular structure of the mixture constituents plays a significant role in the overall mixture selectivity. TOPO emerged as the most effective HBA, demonstrating the highest HBA moment and a negligible HBD moment, which indicates its ability to form robust hydrogen bonds – crucial for optimal process performance.

Based on the COSMO-RS results, twelve mixtures were selected and tested for their density, viscosity, hydrogen bonding interactions, and overall SLM stability. Of these, the TOPO-thymol mixture demonstrated the best stability (with a solvent residual of 78.5%), largely due to its higher viscosity (77.9 cP). In contrast, the lidocaine-based mixtures, despite having a higher viscosity (> 200 cP), exhibited lower stability (< 20%), likely due to greater water solubility and weaker hydrogen bonding. Additionally, the TOPO-based mixtures with long-chained saturated carboxylic acids did not achieve the same stability as TOPO-thymol, due to their lower viscosity (< 50 cP). The TOPO-thymol mixture also delivered high solute fluxes, with values of 9.0±3.0, 16.5±5.4, and 0.7±0.3 g/(m^2h) for MBA, MPPA, and IPA, respectively. These fluxes significantly outperformed the ionic liquid benchmark, which recorded fluxes of 2.7±0.0, 4.9±0.1, and 1.7±0.4 g/(m^2h) for the same compounds. Additionally, the TOPO-thymol mixture showed enhanced selectivity values of 12.4±0.8 and 22.8±1.4 for MBA/IPA and MPPA/IPA, respectively, compared to the organic benchmark undecane, which had selectivity values of 6.9±0.8 and 10.1±1.3. While the COSMO-RS model, based on infinite dilution activity coefficients and assuming mutual phase immiscibility, proved effective for initial screening, the discrepancies between experimental and simulated selectivity values indicate that further analysis is needed for more accurate predictions.

In conclusion, the TOPO-thymol mixture exhibits strong potential as a solvent for SLM extraction of aromatic amines. Critical factors for effective liquid mixtures used include strong HBA or HBD moments to support robust hydrogen bond formation, as well as high viscosity and hydrophobicity. This research contributes to the improvement of current ISPR processes by improving efficiency, reducing environmental impact, and lowering costs in the production of valuable chiral amine compounds. Future studies should investigate the long-term stability and reusability of TOPO-based mixtures under practical conditions and focus on improving their stability. Additionally, since variations in operating conditions were found to affect the overall SLM stability, further investigation is needed. Key parameters to explore include flow rates, temperature, feed concentration, and pH. Last, assessing the scalability of this technology and its integration into existing industrial systems will be crucial for its practical implementation.

Acknowledgement

The authors would like to express their sincere gratitude for the support provided by the Flemish Strategic Basic Research Program under the Catalisti cluster, as well as Flanders Innovation & Entrepreneurship, through the EASiCHEM project (contracts HBC.2018.0484 and K200522N). This research was partially conducted within the framework of the CICECO-Aveiro Institute of Materials project (UIDB/50011/2020, UIDP/50011/2020, and LA/P/0006/2020), with funding from national sources through FCT/MEC (PIDDAC). The authors extend their appreciation to Catherine Echezuria and Amaury Gilles for their valuable contributions to the experimental work in this study.

Declaration of generative AI and AI-assisted technologies in the writing process

During the preparation of this work the authors used ChatGPT in order to assist with language refinement and clarity. After using this tool/service, the authors reviewed and edited the content as needed and takes full responsibility for the content of the publication.

References

[1] W. Khanam, N.C. Dubey, Recent advances in immobilized ω-transaminase for chiral amine synthesis, Mater. Today Chem. 24 (2022) 100922.

[2] J. Yang, A. Buekenhoudt, M. Van Dael, P. Luis, Y. Satyawali, R. Malina, S. Lizin, A techno-economic assessment of a biocatalytic chiral amine production process integrated with *in situ* membrane extraction, Org. Process Res. Dev. 26 (2022) 2052–2066.

[3] Q. Yin, Y. Shi, J. Wang, X. Zhang, Direct catalytic asymmetric synthesis of α-chiral primary amines, Chem. Soc. Rev. 49 (2020) 6141–6153.

[4] A. Cabré, X. Verdaguer, A. Riera, Recent advances in the enantioselective synthesis of chiral amines *via* transition metal-catalyzed asymmetric hydrogenation, Chem. Rev. 122 (2022) 269–339.

[5] J.H. Schrittwieser, S. Velikogne, W. Kroutil, Biocatalytic imine reduction and reductive amination of ketones, Adv. Synth. Catal. 357 (2015) 1655–1685.

[6] J.D. Rozzell, Biocatalysis at commercial scale: myths and realities, Chim. Oggi. 17 (1999) 42–47.

[7] D. Ghislieri, N.J. Turner, Biocatalytic approaches to the synthesis of enantiomerically pure chiral amines, Top Catal. 57 (2014) 284–300.

[8] S. Mathew, D. Renn, M. Rueping, Advances in one-pot chiral amine synthesis enabled by amine transaminase cascades: pushing the boundaries of complexity, ACS Catal. 13 (2023) 5584–5598.

[9] M.D. Patil, G. Grogan, A. Bommarius, H. Yun, Oxidoreductase-catalyzed synthesis of chiral amines, ACS Catal. 8 (2018) 10985–11015.

[10] F. Guo, P. Berglund, Transaminase biocatalysis: optimization and application, Green Chem. 19 (2017) 333–360.

[11] S.A. Kelly, S. Mix, T.S. Moody, B.F. Gilmore, Transaminases for industrial biocatalysis: novel enzyme discovery, Appl. Microbiol. Biotechnol. 104 (2020) 4781–4794.

[12] P. Tufvesson, J. Lima-Ramos, J.S. Jensen, N. Al-Haque, W. Neto, J.M. Woodley, Process considerations for the asymmetric synthesis of chiral amines using transaminases, Biotechnol. Bioeng. 108 (2011) 1479–1493.

[13] T. Börner, G. Rehn, C. Grey, P. Adlercreutz, A process concept for high-purity production of amines by transaminase-catalyzed asymmetric synthesis: combining enzyme cascade and membrane-assisted ISPR, Org. Process Res. Dev. 19 (2015) 793–799.

[14] L. Gianfreda, M.A. Rao, R. Scelza, M. De La Luz Mora, Role of enzymes in environment cleanup/remediation, Elsevier Inc., 2016.

[15] J.S. Shin, B.G. Kim, Asymmetric synthesis of chiral amines with ω-transaminase, Biotechnol. Bioeng. 65 (1999) 206–211.

[16] M. Farah, J. Giralt, F. Stüber, J. Font, A. Fabregat, A. Fortuny, Supported liquid membranes for the removal of pharmaceuticals from aqueous solutions, J. Water Process Eng. 49 (2022) 103170.

[17] Y. Chen, P.O. Saboe, J.S. Kruger, E.C.D. Tan, J.W. Dempsey, J.G. Linger, V. Nogue, E.M. Karp, G.T. Beckham, Liquid-liquid extraction for *in situ* carboxylic acid recovery *via* continuous membrane-based emulsion separations, Green Chem. 26 (2024) 9398-9414.

[18] G. Van Eygen, B. Van der Bruggen, A. Buekenhoudt, P. Luis Alconero, Efficient membrane-based affinity separations for chemical applications: a review, Chem. Eng. Process. 169 (2021) 108613.

[19] J.Ø. Madsen, J.M. Woodley, Considerations for the scale-up of *in vitro* transaminase-catalyzed asymmetric synthesis of chiral amines, ChemCatChem, 15 (2023) e202300560.

[20] P. Dzygieł, P.P. Wieczorek, Supported liquid membranes and their modifications: definition, classification, theory, stability, application and perspectives, in: Liquid Membranes: Principles and Applications in Chemical Separations and Wastewater Treatment, 2009: pp. 73–140.

[21] E. Carasek, J. Merib, Membrane-based microextraction techniques in analytical chemistry: a review, Anal. Chim. Acta 880 (2015) 8–25.

[22] H. Tabani, S. Nojavan, M. Alexovič, J. Sabo, Recent developments in green membrane-based extraction techniques for pharmaceutical and biomedical analysis, J. Pharm. Biomed. Anal. 160 (2018) 244–267.

[23] M.A.R. Martins, S.P. Pinho, J.A.P. Coutinho, Insights into the nature of eutectic and deep eutectic mixtures, J. Solution Chem. 48 (2019) 962–982.

[24] G.M. Martínez, G.G. Townley, R.M. Martínez-Espinosa, Controversy on the toxic nature of deep eutectic solvents and their potential contribution to environmental pollution, Heliyon 8 (2022) e12567.

[25] D. Yu, Z. Xue, T. Mu, Deep eutectic solvents as a green toolbox for synthesis, Cell. Rep. Phys. Sci. 3 (2022) 100809.

[26] P. Kalhor, K. Ghandi, Deep eutectic solvents for pretreatment, extraction, and catalysis of biomass and food waste, Molecules 24 (2019) 4012.

[27] B.B. Hansen, S. Spittle, B. Chen, D. Poe, Y. Zhang, J.M. Klein, A. Horton, L. Adhikari, T. Zelovich, B.W. Doherty, B. Gurkan, E.J. Maginn, A. Ragauskas, M. Dadmun, T.A. Zawodzinski, G.A. Baker, M.E. Tuckerman, R.F. Savinell, J.R. Sangoro, Deep eutectic solvents: a review of fundamentals and applications, Chem. Rev. 121 (2021) 1232–1285.

[28] U. Saeed, A. Laeeq Khan, A. Gilani, M. Aslam, A.U. Khan, CO_2 separation by supported liquid membranes synthesized with natural deep eutectic solvents, Environ. Sci. Pollut. Res. 28 (2021) 33994–34008.

[29] R. Craveiro, L.A. Neves, A.R.C. Duarte, A. Paiva, Supported liquid membranes based on deep eutectic solvents for gas separation processes, Sep. Purif. Technol. 254 (2021) 117593.

[30] K. Xin, P. Zhou, M. van Sint Annaland, Experimental study on CO_2 separation using hydrophobic deep eutectic solvent based supported liquid membranes, Sep. Purif. Technol. 310 (2023) 123129.

[31] M. Xu, H. Dou, F. Peng, N. Yang, X. Xiao, X. Tantai, Y. Sun, B. Jiang, L. Zhang, Ultra-stable copper decorated deep eutectic solvent based supported liquid membranes for olefin/paraffin separation: in-depth study of carrier stability, J. Memb. Sci. 659 (2022) 120775.

[32] B. Jiang, H. Dou, L. Zhang, B. Wang, Y. Sun, H. Yang, Z. Huang, H. Bi, Novel supported liquid membranes based on deep eutectic solvents for olefin-paraffin separation *via* facilitated transport, J. Memb. Sci. 536 (2017) 123–132.

[33] R. Deng, Y. Sun, H. Bi, H. Dou, H. Yang, B. Wang, W. Tao, B. Jiang, Deep eutectic solvents as tuning media dissolving Cu^+ used in facilitated transport supported liquid membrane for ethylene/ethane separation, Energy Fuels 31 (2017) 11146–11155.

[34] T.K. Rye, G. Martinovic, L.V. Eie, F.A. Hansen, T.G. Halvorsen, S. Pedersen-Bjergaard, Electromembrane extraction of peptides using deep eutectic solvents as liquid membrane, Anal. Chim. Acta 1175 (2021) 338717.

[35] C.H.J.T. Dietz, M.C. Kroon, M. Di Stefano, M. Van Sint Annaland, F. Gallucci, Selective separation of furfural and hydroxymethylfurfural from an aqueous solution using a supported hydrophobic deep eutectic solvent liquid membrane, Faraday Discuss 206 (2018) 77–92.

[36] Z. Li, Y. Cui, Y. Shen, C. Li, Extraction process of amino acids with deep eutectic solvents-based supported liquid membranes, Ind. Eng. Chem. Res. 57 (2018) 4407–4419.

[37] A. Klamt, COSMO-RS: from quantum chemistry to fluid phase thermodynamics and drug design, Elsevier B.V., 2005.

[38] A. Klamt, F. Eckert, COSMO-RS: A novel and efficient method for the a priori prediction of thermophysical data of liquids, Fluid Phase Equilib. 172 (2000) 43–72.

[39] A. Klamt, V. Jonas, T. Bürger, J.C.W. Lohrenz, Refinement and parametrization of COSMO-RS, J. Phys. Chem. A 102 (1998) 5074–5085.

[40] A. Klamt, The COSMO and COSMO-RS solvation models, Wiley Interdiscip. Rev. Comput. Mol. Sci. 8 (2018) e1338.

[41] M. Diedenhofen, A. Klamt, COSMO-RS as a tool for property prediction of IL mixtures—a review, Fluid Phase Equilib. 294 (2010) 31–38.

[42] Y. Lyu, J.F. Brennecke, M.A. Stadtherr, Review of recent aromatic-aliphatic-ionic liquid ternary liquid- liquid equilibria and their modeling by COSMO-RS, Ind. Eng. Chem. Res. 59 (2020) 8871–8893.

[43] K. Paduszyński, An overview of the performance of the COSMO-RS approach in predicting the activity coefficients of molecular solutes in ionic liquids and derived properties at infinite dilution, Phys. Chem. Chem. Phys. (2017) 11835-11850.

[44] K. Paduszyński, M. Królikowska, Extensive evaluation of performance of the COSMO-RS approach in capturing liquid-liquid equilibria of binary mixtures of ionic liquids with molecular compounds, Ind. Eng. Chem. Res. 59 (2020) 11851–11863.

[45] J.P. Wojeicchowski, A.M. Ferreira, D.O. Abranches, M.R. Mafra, J.A.P. Coutinho, Using COSMO-RS in the design of deep eutectic solvents for the extraction of antioxidants from rosemary, ACS Sustain. Chem. Eng. 8 (2020) 12132–12141.

[46] M.A. Al-Maari, H.F. Hizaddin, A. Hayyan, M.K. Hadj-Kali, Screening deep eutectic solvents as green extractants for oil from plant seeds based on COSMO-RS model, J. Mol. Liq. 393 (2024).

[47] D. Xu, J. Chow, C.C. Weber, M.A. Packer, S. Baroutian, K. Shahbaz, Evaluation of deep eutectic solvents for the extraction of fucoxanthin from the alga *Tisochrysis lutea* - COSMO-RS screening and experimental validation, J. Environ. Chem. Eng. 10 (2022) 108370.

[48] Z. Salleh, I. Wazeer, S. Mulyono, L. El-blidi, M.A. Hashim, M.K. Hadj-Kali, Efficient removal of benzene from cyclohexane-benzene mixtures using deep eutectic solvents – COSMO-RS screening and experimental validation, J. Chem. Thermodyn. 104 (2017) 33–44.

[49] E. Riveiro, B. González, Á. Domínguez, Extraction of adipic, levulinic and succinic acids from water using TOPO-based deep eutectic solvents, Sep. Purif. Technol. 241 (2020) 116692.

[50] A. Kshirsagar, P.K. Verma, M.S. Murali, New hydrophobic DES based on tri–n-octylphosphine oxide and dicarboxylic acids: synthesis, spectroscopy and liquid–liquid extraction of actinides, J. Radioanal. Nucl. Chem. 330 (2021) 1053–1064.

[51] S.J.R. Vargas, G. Pérez-Sánchez, N. Schaeffer, J.A.P. Coutinho, Solvent extraction in extended hydrogen bonded fluids - separation of Pt(IV) from Pd(II) using TOPO-based type V DES, Green Chem. 23 (2021) 4540–4550.

[52] J. Gamare, B.G. Vats, A hydrophobic deep eutectic solvent for nuclear fuel cycle: Extraction of actinides and dissolution of uranium oxide, Eur. J. Inorg. Chem. 26 (2023) e202300441.

[53] P. Makoś, E. Słupek, J. Gębicki, Hydrophobic deep eutectic solvents in microextraction techniques – a review, Microchem. J. 152 (2020) 104384.

[54] J. Cao, E. Su, Hydrophobic deep eutectic solvents: The new generation of green solvents for diversified and colorful applications in green chemistry, J. Clean Prod. 314 (2021) 127965.

[55] Q. Qu, Y. Lv, L. Liu, K.H. Row, T. Zhu, Synthesis and characterization of deep eutectic solvents (five hydrophilic and three hydrophobic), and hydrophobic application for microextraction of environmental water samples, Anal. Bioanal. Chem. 411 (2019) 7489–7498.

[56] C. Florindo, F.S. Oliveira, L.P.N. Rebelo, A.M. Fernandes, I.M. Marrucho, Insights into the synthesis and properties of deep eutectic solvents based on cholinium chloride and carboxylic acids, ACS Sustain. Chem. Eng. 2 (2014) 2416–2425.

[57] G. Van Eygen, S. Keuppens, X. De Breuck, B. Swankaert, P. Boura, E. Loccufier, J. Kosek, D. Ramasamy, F. Nahra, A. Buekenhoudt, K. De Clerck, B. Van der Bruggen, P. Luis, Comparison of distinctive polymeric membrane structures as support materials for membrane extraction of chiral amines, Sep. Purif. Technol. 352 (2025) 128192.

[58] G. Van Eygen, D. Mariën, A. Vananroye, C. Clasen, B. Van der Bruggen, A. Buekenhoudt, J.A.P. Coutinho, P. Luis, Facilitated solvent screening for membrane-based extraction of chiral amines *via* a priori simulations, J. Mol. Liq. 375 (2023) 121351.

[59] Z. Zhang, R. Lu, Q. Zhang, J. Chen, W. Li, COSMO-RS based ionic liquid screening for the separation of acetonitrile and ethanol azeotropic mixture, J. Chem. Technol. Biot. (2020) 1191-1202..

[60] H.W. Khan, A.V.B. Reddy, M.M.E. Nasef, M.A. Bustam, M. Goto, M. Moniruzzaman, Screening of ionic liquids for the extraction of biologically active compounds using emulsion liquid membrane: COSMO-RS prediction and experiments, J. Mol. Liq. (2020) 113122.

[61] J.P. Wojeicchowski, C. Marques, L. Igarashi-Mafra, J.A.P. Coutinho, M.R. Mafra, Extraction of phenolic compounds from rosemary using choline chloride – based Deep Eutectic Solvents, Sep. Purif. Technol. (2021) 117975.

[62] A. Cicci, M. Bravi, Leveraging novel green solvents to drive conceptual and practical biorefinery innovation, in: Studies in Surface Science and Catalysis, Vol. 179, Elsevier, 2020, pp. 243-259.

[63] M. Terasaki, R. Abe, M. Makino, N. Tatarazako, Chronic toxicity of parabens and their chlorinated by-products in *Ceriodaphnia dubia*, Environ. Toxicol. 30 (2015) 664–673.

[64] D. Vearrier, D. Jacobs, M.I. Greenberg, Phenol toxicity following cutaneous exposure to creolin®: a case report, J. Med. Toxicol. 11 (2015) 227–231.

[65] N. Soszka, B. Hachuła, M. Tarnacka, E. Kamińska, J. Grelska, K. Jurkiewicz, M. Geppert-Rybczyńska, R. Wrzalik, K. Grzybowska, S. Pawlus, M. Paluch, K. Kamiński, The impact of the length of alkyl chain on the behavior of benzyl alcohol homologues-the interplay between dispersive and hydrogen bond interactions, Phys. Chem. Chem. Phys. 23 (2021) 23796–23807.

[66] K.A. Kurnia, C.M.S.S. Neves, M.G. Freire, L.M.N.B.F. Santos, J.A.P. Coutinho, Comprehensive study on the impact of the cation alkyl side chain length on the solubility of water in ionic liquids, J. Mol. Liq. (2015) 264-271.

[67] Z. Song, J. Zhang, Q. Zeng, H. Cheng, L. Chen, Z. Qi, Effect of cation alkyl chain length on liquid-liquid equilibria of {ionic liquids + thiophene + heptane}: COSMO-RS prediction and experimental verification, Fluid Phase Equilib. (2016) 244-251.

[68] M. Devi, R. Moral, S. Thakuria, A. Mitra, S. Paul, Hydrophobic deep eutectic solvents as greener substitutes for conventional extraction media: examples and techniques, ACS Omega 8 (2023) 9702–9728.

[69] R.J. Nunes, B. Saramago, I.M. Marrucho, Surface tension of DL-menthol:octanoic acid eutectic mixtures, J. Chem. Eng. Data 64 (2019) 4915–4923.

[70] W. Cui, J. Yan, J. Yang, Y. Wang, X. Wang, Effect of hydrocarbon structure on viscosity reduction of long chain viscoelastic surfactant, J. Mol. Liq. 311 (2020) 113197.

[71] N. Schaeffer, J.H.F. Conceica¸õ, M.A.R. Martins, M.C. Neves, G. Pérez-Sánchez, J.R.B. Gomes, N. Papaiconomou, J.A.P. Coutinho, Non-ionic hydrophobic eutectics-versatile solvents for tailored metal separation and valorisation, Green Chem. 22 (2020) 2810–2820.

[72] N.F. Gajardo-Parra, V.P. Cotroneo-figueroa, P. Aravena, V. Vesovic, R.I. Canales, Viscosity of choline chloride-based deep eutectic solvents: experiments and modeling, J. Chem. Eng. Data 65 (2020) 5581–5592.

[73] D.J.G.P. Van Osch, L.F. Zubeir, A. Van Den Bruinhorst, M.A.A. Rocha, M.C. Kroon, Hydrophobic deep eutectic solvents as water-immiscible extractants, Green Chem. 17 (2015) 4518–4521.

[74] S.W. Kuo, C.F. Huang, F.C. Chang, Study of hydrogen-bonding strength in poly(ε-caprolactone) blends by DSC and FTIR, J. Polym. Sci. B Polym. Phys. 39 (2001) 1348–1359.

[75] L. Guo, H. Sato, T. Hashimoto, Y. Ozaki, FTIR study on hydrogen-bonding interactions in biodegradable polymer blends of poly(3-hydroxybutyrate) and poly(4-vinylphenol), Macromolecules 43 (2010) 3897–3902.

[76] Y. Hirashima, H. Sato, A. Suzuki, ATR-FTIR spectroscopic study on hydrogen bonding of poly(N-isopropylacrylamide-co-sodium acrylate) gel, Macromolecules 38 (2005) 9280–9286.

[77] X. Sheng, X. Jiang, H. Zhao, D. Wan, Y. Liu, C.A. Ngwenya, L. Du, FTIR study of hydrogen bonding interaction between fluorinated alcohol and unsaturated esters, Spectrochim. Acta A Mol. Biomol. Spectrosc. 198 (2018) 239–247.

[78] B. Behera, P. Das, Blue- and red-shifting hydrogen bonding: a gas phase FTIR and *ab Initio* study of RR'CO.DCCl3 and RR'S.DCCl3 complexes, J. Phys. Chem. A 122 (2018) 4481–4489.

[79] J. Coates, Interpretation of infrared spectra, a practical approach, in: Encyclopedia of Analytical Chemistry, John Wiley & Sons Ltd., Chichester, 2000, pp. 10815–10837.

[80] T. Quaid, T. Reza, COSMO prediction of siloxane compounds absorption on type 3 and type 5 deep eutectic solvents, Chem. Eng. J. Adv. 14 (2023) 100489.

[81] K.A. Kurnia, J.A.P. Coutinho, Overview of the excess enthalpies of the binary mixtures composed of molecular solvents and ionic liquids and their modeling using COSMO-RS, Ind. Eng. Chem. Res. 52 (2013) 13862–13874.

[82] H. Cheng, J. Li, J. Wang, L. Chen, Z. Qi, Enhanced vitamin E extraction selectivity from deodorizer distillate by a biphasic system: a COSMO-RS and experimental study, ACS Sustain. Chem. Eng. 6 (2018) 5547–5554.

[83] F.S. Mjalli, O. Ahmad, Density of aqueous choline chloride-based ionic liquids analogues, Thermochim. Acta 647 (2017) 8–14.

[84] A. Pandey, S. Pandey, Solvatochromic probe behavior within choline chloride-based deep eutectic solvents: effect of temperature and water, J. Phys. Chem. B 118 (2014) 14652–14661.

[85] C. Florindo, L.C. Branco, I.M. Marrucho, Development of hydrophobic deep eutectic solvents for extraction of pesticides from aqueous environments, Fluid Phase Equilib. 448 (2017) 135–142.

[86] D.J.G.P. Van Osch, C.H.J.T. Dietz, J. Van Spronsen, M.C. Kroon, F. Gallucci, M. Van Sint Annaland, R. Tuinier, A search for natural hydrophobic deep eutectic solvents based on natural components, ACS Sustain. Chem. Eng. 7 (2019) 2933–2942.

[87] S. Ni, J. Su, H. Zhang, Z. Zeng, H. Zhi, X. Sun, A cleaner strategy for comprehensive recovery of waste SmCo magnets based on deep eutectic solvents, Chem. Eng. J. 412 (2021) 128602.

[88] S. Eid, T. Lemaoui, A.S. Darwish, M.A. Jaoude, F. Banat, S.W. Hasan, I.M. AlNashef, Rapid and highly efficient removal of aqueous perfluorooctanoic acid using deep eutectic solvents for sustainable water remediation: an integrated experimental-modeling approach, Chem. Eng. J. 495 (2024) 153668.

[89] G. Rehn, B. Ayres, P. Adlercreutz, C. Grey, An improved process for biocatalytic asymmetric amine synthesis by *in situ* product removal using a supported liquid membrane, J. Mol. Catal. B Enzym. 123 (2016) 1–7.

[90] P. Dzygieł, P. Wieczorek, P. Kafarski, Supported liquid membrane separation of amine and amino acid derivatives with chiral esters of phosphoric acids as carriers, J. Sep. Sci. 26 (2003) 1050–1056.

Highlights:

- TOPO-thymol mixture shows superior selectivity for aromatic amine extraction.
- COSMO-RS simulations screened over 200 mixtures for SLM extraction effectiveness.
- TOPO's strong HBA moment is crucial for robust hydrogen bond formation.
- High viscosity and hydrophobicity are key for stable and effective SLM extraction.
- TOPO-thymol's success suggests potential for efficient industrial ISPR.

Declaration of interests

☒ The authors declare that they have no known competing financial interests or personal relationships that could have appeared to influence the work reported in this paper.

☐The authors declare the following financial interests/personal relationships which may be considered as potential competing interests: